Finite element modelling of push-out tests for novel Locking Nut Shear Connectors

E.Tzouka[1], T.Karavasilis[2], M.M.Kashani[1], S.Afshan[1]

[1]Faculty of Engineering and Physical Sciences, University of Southampton, Bolderwood Innovation Campus, Burgess Road, Southampton, SO16 7QF, UK

[2]Department of Civil Engineering, University of Patras, 26500, Patras, Greece

Abstract

Steel-concrete composite beams have been used in bridge construction for decades. Novel demountable bolted shear connectors, that allow bridge disassembly and offer high level of prefabrication, are proposed for the connection of the deck with the steel beams, as an alternative to the conventional headed studs. In terms of sustainability, bolted shear connectors facilitate the replacement of deteriorating bridge components and therefore extend the bridge design life. Despite their effectiveness, research on steel-concrete composite beams with bolted shear connectors is limited. In order to expand the available literature, this paper develops a three-dimensional finite element model to investigate the behaviour of a novel demountable shear connector for precast steel-concrete composite bridges. The connector uses high-strength steel bolts, which are fastened to the steel beam with the aid of a special locking nut configuration that prevents the slip of the bolts within their holes. The accuracy of the proposed FE model is validated by comparing its predictions with the experimental results available in the literature. Once validated, the FE model was then used to conduct a parametric study to evaluate the effect of bolt height, diameter and tensile strength, bolt pretension and the compressive strength of concrete on the load-slip behaviour, the shear resistance, the slip capacity and the stiffness of the shear connectors.

Keywords

Bolt connector; Bridge disassembly; Demountable steel-concrete composite bridges; Finite element analysis; High strength bolts; Push-out tests; Shear connectors

1 Introduction

Europe is connected through one of the densest and most developed transport infrastructure networks in the world. However, many European bridges are more than 50 years old. The majority of those bridges are operational today, but their safety is questioned since they have reached the end of their design life and in many cases, they are not well maintained. Durability issues related with corrosion and fatigue are also very common in bridges [1, 2]. Consequently, many EU countries must invest in rehabilitation projects to ensure serviceability and safety. Rehabilitation projects involve inspection, repair and strengthening of the bridge components and often their replacement, if necessary. These operations usually lead to huge economic losses, while invoking long-lasting disruption of the traffic flow [3].

. The deterioration of bridge decks is a major cause of loss of strength and potential failure in bridges. In case of steel-concrete composite bridges, removing and replacing the deteriorating deck is a challenging process due to the connection between the deck and the steel beam. The connection is usually achieved through use of conventional headed studs, which are welded to the top flange of the steel beam and are fully embedded within the concrete deck. Therefore, removing the deck involves drilling and crushing the concrete around the shear connectors and then breaking the deck into manageable sections [4]. Compared with conventional headed studs, bolted shear connectors allow the easy dismantling and rapid replacement of the deteriorating deck. In this way, bolted shear connectors also facilitate the prefabrication of composite beams which reduce the onsite construction time and cost. In terms of sustainable

development, by using bolted shear connectors in composite beams, the steel girders could be recycled and reused at the end of their service life.

Bolted shear connectors in steel-concrete composite structures are rarely used, mainly because of the limited research on their behaviour and the lack of codified design rules. Dallam et al. [5] and Dallam and Harpster [6] conducted experimental studies on high strength friction grip bolts that were embedded in concrete slabs. Subsequently, Kwon et al. [7, 8] examined the use of high-strength bolts as post-installed shear connectors for strengthening existing non-composite bridges. Pavlović et al. [9] investigated the use of bolted shear connectors with single embedded nut in prefabricated concrete slabs in order to achieve higher level of prefabrication in steel concrete composite structures. Dai et al. [10] conducted a series of push-out test in order to evaluate the behaviour of bolted connectors machined from standard welded studs. A number of research studies were conducted on high-strength friction grip bolts with precast concrete slabs by Lee and Bradford [11], Rowe and Bradford [12], Bradford and Pi [13], Ataei and Bradford [14, 15], Chen et al. [16] and Liu et al. [17, 18].

Previous experimental and numerical studies highlighted a major problem in bolted shear connectors. An undesirable large slip of the bolts inside the bolt holes was observed when friction resistance developing along the interface forming between the steel flanges and the concrete slab was exceeded. Furthermore, the shear connectors that are fully embedded in the concrete slab, can only be used for the in-situ construction and therefore are not suitable for precast construction, since very high tolerances need to be overcome to align the pre-embedded bolts in the concrete slab with the corresponding holes on the steel flange. In addition, the shear connectors that are fully embedded in the concrete slab do not allow the full disassembly of the composite beam, since only the slab as a whole can be uplifted and replaced and the replacement of the shear connectors is not possible. Finally, many of the previously proposed bolted shear connectors require the installer to work underneath the bridge to fasten the bolts,

which is considered to be an unfavourable practice. Suwaed and Karavasilis [19] proposed a novel demountable shear connector (Locking Nut Shear Connector – LNSC) for steel-concrete composite bridges that prevents bolt sliding with the aid of a special locking nut configuration and allows fully bridge disassembly. The experimental results showed that the proposed shear connector provide higher resistance and stiffness to the connection compared to conventional welded headed studs and offers improved slip capacity.

The shear behaviour of the LNSC in composite structures has been investigated experimentally by means of push-out tests [19]. Although push-out test are widely used for investigating the behaviour of shear connections, they are often costly and time-consuming. Therefore, the main objective of this paper is to develop an accurate and efficient three-dimensional (3D) finite element (FE) model capable to provide further insight into the behaviour of the LNSCs in steel-concrete composite structures. In the first part of the paper, the developed FE model is presented. To validate the model, the results obtained from the FE analysis are verified against the experimental results from the push-out tests [19]. Subsequently, extensive parametric studies are performed to evaluate the effect of key parameters on the capacity and behaviour of bolted shear connectors. The parameters tested are the bolt pretension force, the diameter, the tensile strength and the height to diameter ratio of the bolt connectors, and the compressive strength of the concrete. Finally, some simple design rules are proposed.

2 Finite element modelling

A three-dimensional (3D) finite element (FE) model was developed using the commercial software ABAQUS to simulate the behaviour of the LNSC in push-out tests. The load-slip behaviour of the push-out tests conducted by Suwaed and Karavasilis [19] was used to validate the FE model.

2.1 Summary of literature push-out tests

The details of the push-out tests, including the bolts diameter, the compressive and tensile strengths of the slab and plugs and compressive strength of the grout, used in the validation of the FE model, are given in Table 1. The test number refers to the corresponding test number of the experimental analysis conducted by Suwaed and Karavasilis [19]. The test set-up and the geometry of the push out specimens are shown in Fig. 1. The tested LNSCs consist of a pair of high-strength steel bolts, which are fastened to the top flange of the beam using a double nut configuration, which consists of a standard lower hexagonal nut and an upper conical nut. The steel beam is a 254×254×89 UC section with a length equal to 700mm. Four holes were drilled on the beam flanges in order to accommodate the high strength bolts along with their conical nuts. The upper part of the bolt holes is a countersunk seat with chamfered sides following an angle of 60°. The geometry of the upper conical nut follows the same angle so that it can perfectly fit within the countersunk seat. In this way, the conical nut prevents the slip of the bolts within their holes by providing a mechanical stop within the countersunk seat. Subsequently, the lower hexagonal nuts were tightened to securely lock the bolts within their holes.

The geometry of the slabs is 650×600×150mm with a central countersunk conical pocket to accommodate the shear connector. Rapid hardening grout was poured into the slab pockets and then a precast plug was placed around each bolt and gradually inserted into the slab pocket. A hardened plate washer was used to uniformly distribute the bolt thrust on the upper face of the

concrete plug without inducing cracks. Finally, the tightening of the upper hexagonal nut was performed before the hardening of the grout to avoid developing internal stresses in the slab.

Table 1. Specifications of the push-out tests

Test Number	Bolt Diameter (mm)	Slab		Plugs		Grout
		Compressive Strength (MPa)	Tensile Strength (MPa)	Compressive Strength (MPa)	Tensile Strength (MPa)	Compressive Strength (MPa)
7	12	50	4	91	4.8	28
8	14	50	4	95	4.6	32
10	16	43	3.1	50	3.7	27
12	16	42	3.5	91	4.9	28

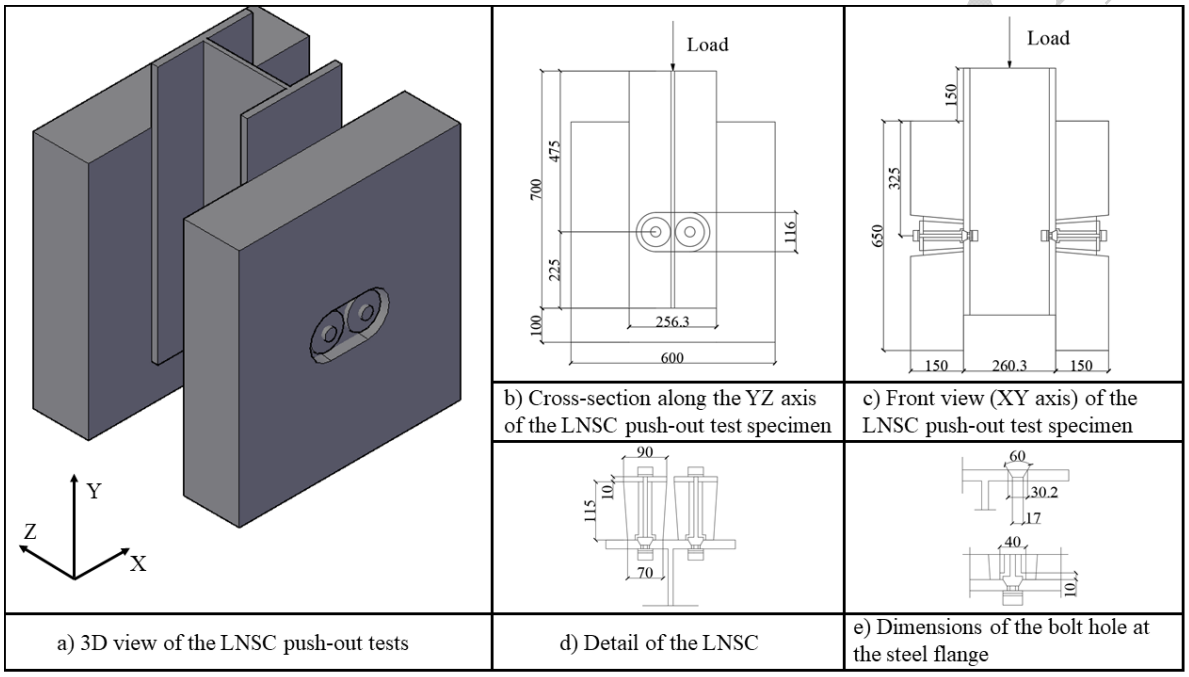

a) 3D view of the LNSC push-out tests

b) Cross-section along the YZ axis of the LNSC push-out test specimen

c) Front view (XY axis) of the LNSC push-out test specimen

d) Detail of the LNSC

e) Dimensions of the bolt hole at the steel flange

Fig. 1. Details of the push-out specimens with LNSC connectors (Dimensions are given in mm).

2.2 Development of numerical models

2.2.1 Geometry and mesh

The FE model consisted of all connection components used in the push-out tests to accurately predict the behaviour of the LNSC: steel beam, precast concrete plugs and slabs, high-strength bolts, plate washers, grout and steel reinforcement. High-strength bolts, hexagonal nuts, washers and conical nut were modelled as one part to avoid convergence difficulties due to complicated contact interactions. One quarter of the push-out test arrangement was modelled using double vertical symmetry condition. The precast concrete parts of the LNSC, the steel beam and the high-strength bolts were modelled using three-dimensional eight node linear hexahedral solid elements with reduced integration and hourglass control (C3D8R). Elements with reduced integration were adopted as they could reduce the computational time and improve the convergence rate. The reinforcing bars were modelled with two node linear three-dimensional truss elements (T3D2). The mesh sizes adopted for the different components of the LNSC are shown in Fig. 2. To reduce the computational time, a coarse mesh was adopted for the overall push-out specimen, with a fine mesh being used for the region around the shear connector to improve the accuracy of the model. The mesh size ranges from 2mm for high-strength bolts to 8mm for precast concrete slabs. Following a mesh sensitivity analysis, the adopted mesh sizes were found to give optimum accuracy and computational efficiency.

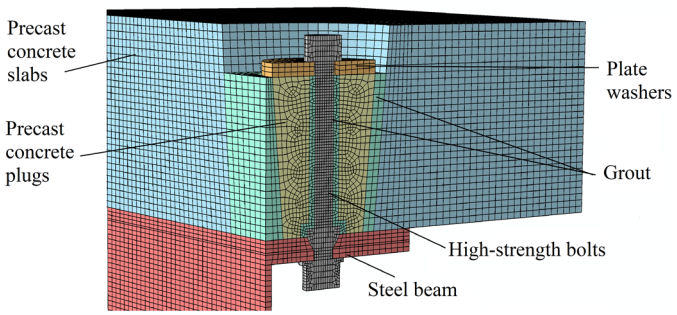

Fig. 2. Mesh of LNSC push-out tests.

2.2.2 Interactions and Boundary Conditions

The interactions between the various components of the LNSC push-out specimens were modelled using appropriate interaction and constraint conditions available in ABAQUS software. The surface-to-surface contact interaction was applied at all the interfaces in the model, by using the 'Hard' and 'Penalty' options to describe the normal and tangential behaviour between the contact surfaces respectively. A friction coefficient equal to 0.45 was used for the contact interaction between the steel and concrete components, while the friction coefficient was taken as 0.25 for the contact interaction between the steel beam and high-strength bolts [18]. The embedded constraint option was applied to the reinforcement bars and concrete slab, in order to constrain the translational DOF of the nodes on the rebar elements to the interpolated values of the corresponding DOF of the concrete elements.

The boundary conditions used in the FE analysis are presented in Fig. 3. For the quarter models, two planes of symmetry were taken into consideration – Surface 1 and Surface 2. Surface 1 was restrained from translating in the Z direction and rotating in the X and Y directions, while Surface 2 was restrained from translating in the X direction and rotating in the Y and Z directions. All nodes at the bottom end of the concrete slab (Surface 3) were restrained against all translational and rotational degrees of freedom.

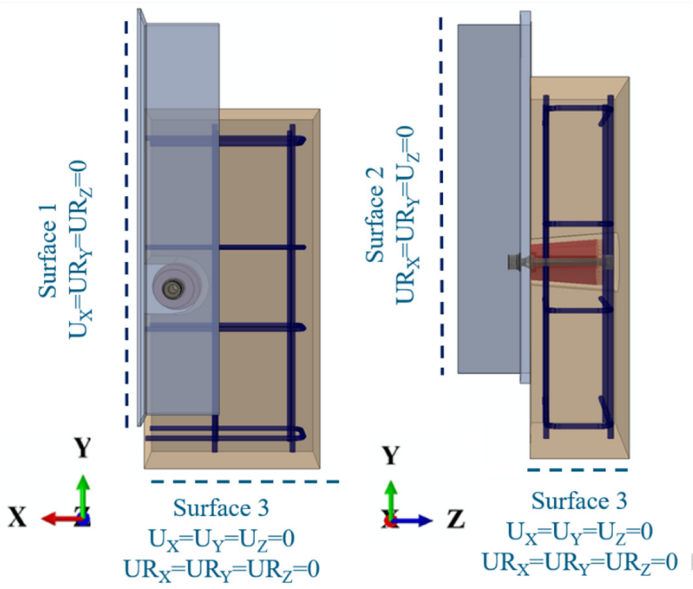

Fig. 3. Boundary conditions.

2.2.3 Material Properties

2.2.3.1 Steel

The bilinear plus nonlinear hardening model proposed by Yun et al. [20] was used to represent the material stress-strain behaviour of the steel beam. The material behaviour was defined in three distinct phases using Eq. (1). The material behaviour is linear up to the yield stress f_y and the corresponding yield strain ε_y, followed by a region of plastic flow at an approximate constant stress until the stain-hardening strain ε_{sh} is reached. After this point, stress accumulation recommences at a reducing rate up to the ultimate stress f_u and the corresponding ultimate tensile strain ε_u.

$$f(\varepsilon) = \begin{cases} E\varepsilon, & for\ \varepsilon \le \varepsilon_y \\ f_y, & for\ \varepsilon_y < \varepsilon \le \varepsilon_{sh} \\ f_y + (f_u - f_y)\left[\dfrac{0.4c + 2c}{(1 + 400c^5)^{1/5}}\right], & for\ \varepsilon_{sh} < \varepsilon \le \varepsilon_u \end{cases} \quad (1)$$

Where

$$c = (\varepsilon - \varepsilon_{sh})/(\varepsilon_u - \varepsilon_{sh}) \quad (2)$$

For the steel reinforcement, a simple elastic-perfectly plastic model, without strain hardening, and yield strength equal to 500MPa was employed [21]. The stress-strain relationships for both steel beam and steel reinforcement are shown in Fig.4.

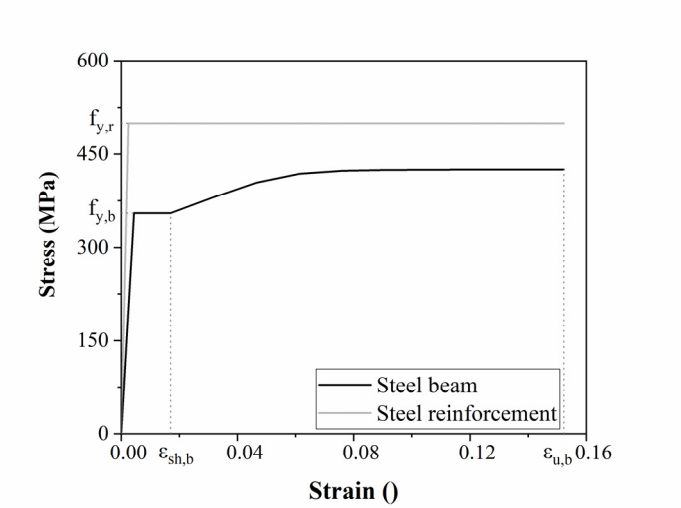

Fig. 4. Stress strain relationship for steel beam and steel reinforcement.

Isotropic plasticity with initial modulus of elasticity $E = 210\ GPa$ and Poisson's ratio $v = 0.3$ was used for high-strength bolt connectors. Ductile damage models were included in the analysis to investigate the failure of the bolts. Parameters of ductile damage initiation criterions and damage evolution laws were derived by using data obtained from standard tensile tests conducted by Suwaed and Karavasilis [19]. Standard tensile test models were built in ABAQUS software and damage parameters were calibrated by comparing numerical and experimental results.

A damage initiation criterion was used in the FE model to define the onset of damage. The damage initiation criterion used assumes that the equivalent plastic strain at the onset of damage, $\bar{\varepsilon}_0^{pl}$, is a function of stress triaxiality, η, and strain rate, $\dot{\bar{\varepsilon}}^{pl}$. Pavlovic et al. [9] proposed Eq. (3) based on experimental and theoretical findings of Trattnig [22] and Rice and Tracey [23], to define the dependency of the equivalent plastic strain at the onset of damage on stress triaxiality.

$$\bar{\varepsilon}_0^{pl} = \varepsilon_n^{pl} exp\left[-\beta\left(\eta - \frac{1}{3}\right)\right] \quad (3)$$

Material parameter $\beta = 1.5$ was adopted, as proposed by Rice and Tracey [23]. The uniaxial true plastic strain at the onset of necking, $\varepsilon_n^{pl} = 0.07118$, was obtained from the standard tensile test results [19].

After the onset of damage, Hillerborg's theory [24] was used to reduce the mesh dependency of the results due to strain localization. With this approach, the behaviour of the material was described in terms of fracture energy. A scalar damage variable, D, was induced in the model to account for the stiffness degradation of the material. At any given time during the analysis, the scalar damage variable is given by Eq. (4):

$$D = 1 - \frac{\sigma}{\bar{\sigma}} \quad (4)$$

where σ is the stress tensor computed in the current increment and $\bar{\sigma}$ are the stresses that would exist in the material in the absence of damage. In order to define the undamaged response of the material, the stresses after the point of damage initiation were assumed to rise linearly following the same slope as right before the damage was initiated.

The progressive damage degradation of high-strength bolts was described by using a scalar damage variable D. The damage variable was given as a tabular function of the equivalent plastic displacement u^{pl}. The equivalent plastic displacement at fracture, u_f^{pl}, defined by running the model without the damage initiation criterion. The average value of the equivalent plastic strain at the elements that are expected to fail was measured at the time increment when the final fracture was expected to happen. The value was then used to calculate the equivalent plastic displacement at failure using Eq. (5).

$$\dot{u}_f^{pl} = L\dot{\varepsilon}_f^{pl} \tag{5}$$

where L accounts for the characteristic length, which depends on the element geometry and formulation. Subsequently, the input data for damage evolution law were calibrated using an iterative procedure until the force-displacement curve matched the experimental results.

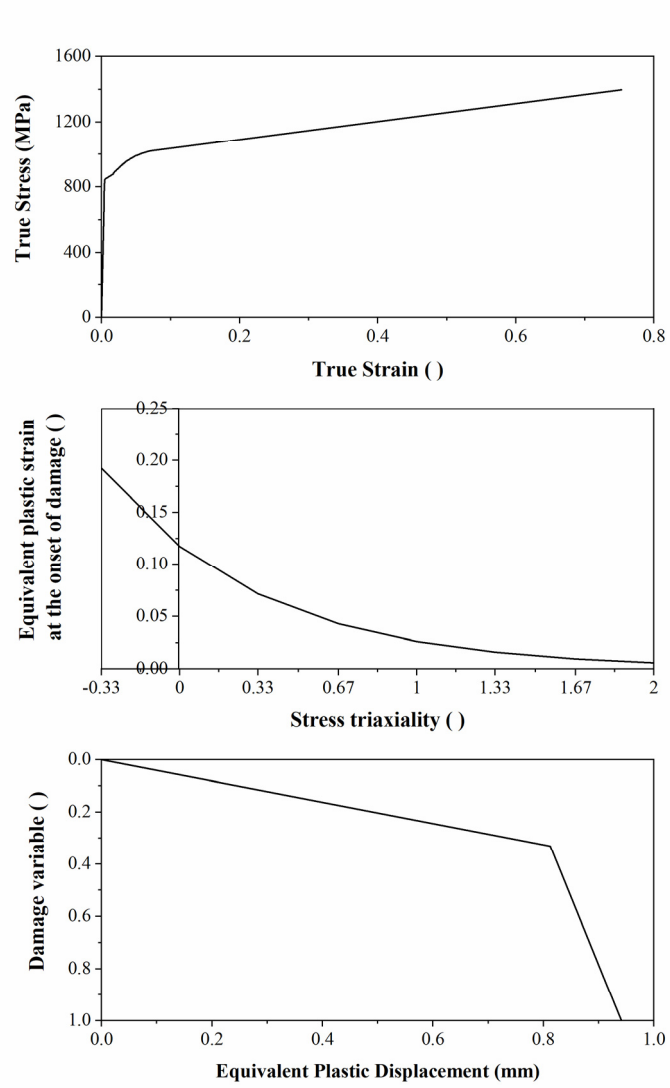

Fig. 5. Stress-strain relationship and ductile damage parameters for high-strength bolts.

The results obtained from the FE model of the tensile tests are compared against the experimental data [19] in Fig. 6. The FE model predicted the load-displacement response of the tensile specimens as well as the stiffness degradation of the material. As shown in Fig.7 the strains are localized at the centre of the specimens and form a “necking region”.

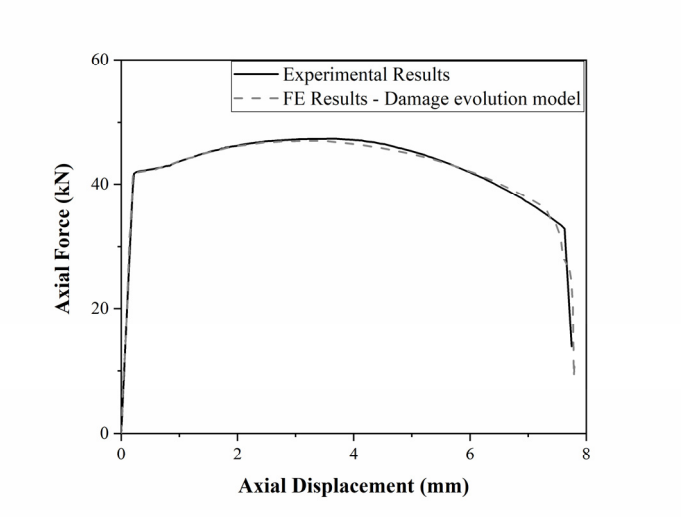

Fig. 6. Experimental [19] and numerical force-displacement response of standard tensile test specimens.

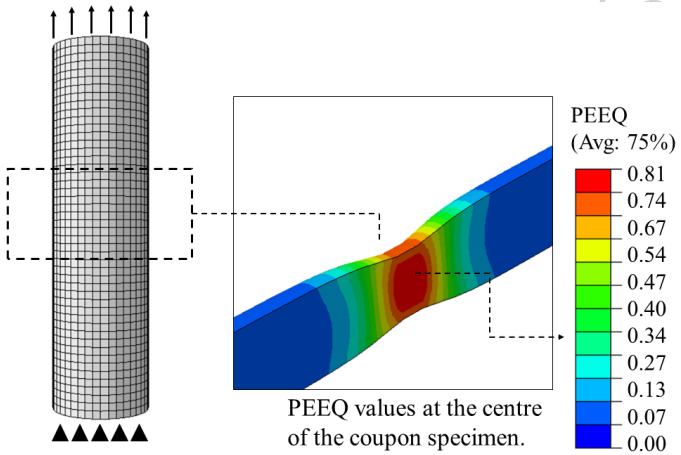

Fig. 7. Localized strains and formation of a "necking" region at the centre of the coupon specimens.

2.2.3.2 Concrete Properties

Concrete Damage Plasticity (CDP) model was employed to simulate the behaviour of the concrete components of the LNSC; precast concrete plugs, precast concrete slabs and grout. CDP uses the concepts of isotropic damaged elasticity in combination with isotropic tensile and compressive plasticity to represent the inelastic behaviour of concrete. The mechanical properties of the plugs, slabs and grout are presented in Table 1.

The uniaxial stress-strain relationship proposed by Carreira & Chu [25] was used for precast concrete slabs and grout in compression. The compressive behaviour of the precast concrete plugs was defined by using the modified uniaxial stress-strain relationship for high strength concrete proposed by Hsu & Hsu [26].

According to the experimental investigation conducted by Suwaed and Karavasilis [19], the part of the concrete plug in front of the conical nut is under nearly triaxial stress confinement conditions due to the pretensioning of upper hexagonal nut. Concrete is significantly stronger in triaxial compression, and as Oehlers and Bradford [27] estimated, the concrete adjacent to the collar of the welded stud can withstand 7.0 times its cylinder strength. Therefore, precast concrete plugs can develop stresses higher that their 80-100MPa design strength.

To take into account the complex nature of passively confined concrete, key material parameters were determined; the ratio of the second stress invariant on the tensile meridian to that on the compressive meridian (K_c), dilation angle (ψ), flow potential eccentricity (e), and the ratio of the compressive strength under biaxial loading to uniaxial compressive strength (f_{b0}/f_c'). Papanikolaou and Kappos [28], proposed Eq. (6) to determine the ratio of f_{b0}/f_c'.

$$\frac{f_{b0}}{f_c'} = 1.5\,(f_c')^{-0.075} \tag{6}$$

Yu et al.[29] proposed Eq. (7) in order to express K_c as a function of the compressive strength of the concrete.

$$K_c = \frac{5.5}{5 + 2(f_c')^{0.075}} \quad (7)$$

A value of e = 0.1 was adopted for the flow potential eccentricity, according to ABAQUS user manual recommendations [30]. Dilation angle values were iteratively calibrated to match push-out tests results.

Scalar damage variables presented in Eq. (8-9) were included in the FE model to account for compression and tension damage of the concrete parts of the connector.

$$D_c = 1 - \sigma_c / f_c \quad (8)$$

$$D_t = 1 - \sigma_t / f_t \quad (9)$$

The tensile behaviour of concrete was assumed to be linear until its ultimate tensile strength. After this point, Hillerborg's [24] fracture energy approach was adopted in order to minimize the mesh sensitivity of the results. Hillerborg used Eq. (10) to define the energy required to open a unit area of crack as a material parameter, using brittle fracture concepts.

$$G_f = (0.0468 {d_{max}}^2 - 0.5 d_{max} + 26) {f_t}^{0.7} \quad (10)$$

Where f_t is in MPa and d_{max} is the maximum coarse aggregate size (in mm).

Using this approach, the tensile softening response of concrete was characterized by means of fracture energy [31],[32]. A linear loss of strength was assumed in this model as shown in Fig. 8 [30].

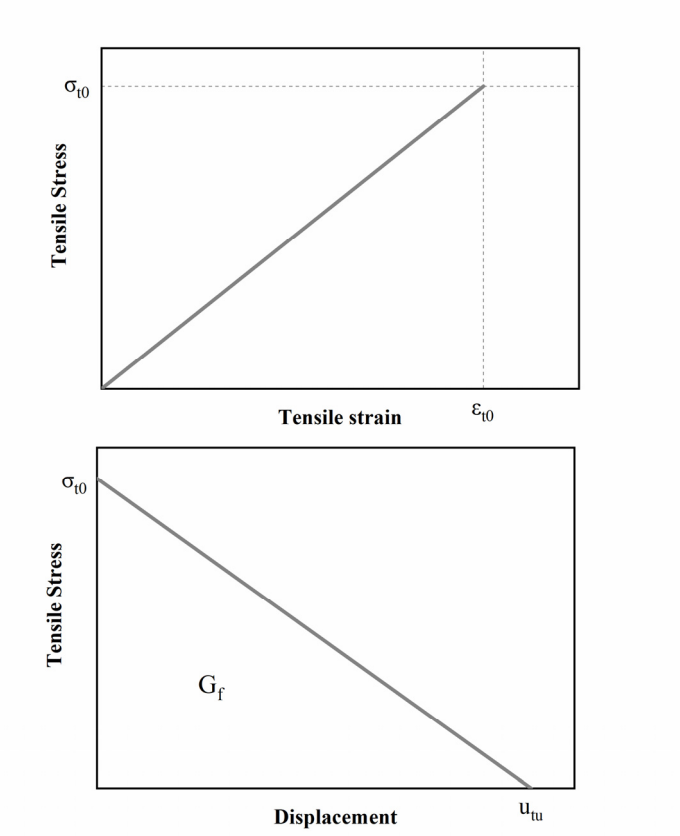

Fig. 8. Concrete behaviour in tension.

2.2.4 Analysis Procedure

A quasi-static analysis was performed using the ABAQUS/Explicit solver to allow for the use of damage and failure models with element deletion in the models. The explicit dynamic analysis method is suitable for models with complex geometries and contact interactions, for which the implicit formulation usually encounters convergence issues [30]. The mass of the model was increased artificially by using the mass scaling option with time increment of 0.00001 sec for computational efficiency. Both kinetic and internal energy were monitored throughout the analysis, to ensure that the quasi-static conditions are maintained; the kinetic energy was less than 5% of the internal energy.

The loading was defined in two steps, corresponding to the experimental testing. In the first step of the analysis, the pre-tensioning of the high-strength bolts was simulated by using the predefined temperature field option. The desired temperature value was calibrated to ensure a

good agreement between the applied and actual stresses on the bolts. A prescribed push down displacement was applied on the upper edge of the beam flange, along the U_y direction as shown in Fig. 3, on the second step of the analysis.

2.3 Validation of numerical results

Load-slip response, deformation/damage patterns and failure modes of the specimens were predicted and verified against the experimental results [19]. The specifications of the push-out specimens used for the validation of the FE model are presented in Table 1. The load-slip response of the push-out specimens with LNSC are compared with the FE predictions in Fig. 9 and a relatively good agreement between the predicted and the experimental curves is observed.

The FE model was capable of predicting the load-slip response characteristics exhibited by the LNSC. Initially, the shear-load slip response is linear up to about 20% of the ultimate shear resistance of the LNSC. The applied forces are transmitted smoothly from steel beam to the concrete slabs through friction resistance at the interface. As the applied force increases, the friction resistance of LNSC is overcome and the bolted connection starts resisting shear force through bearing. The response of the shear connectors becomes nonlinear with the gradual yielding of the bolts and crushing of the grout in front of the conical nut and the bolt shank. As the shear load reaches its maximum values, the conical nut and the bolt shank start to bear against the precast concrete plug. As a result, the concrete shear strains in the part of the plug that is in front of the conical nut increase and a concrete shear failure plane forms which passes through the grout-plug-slab interface.

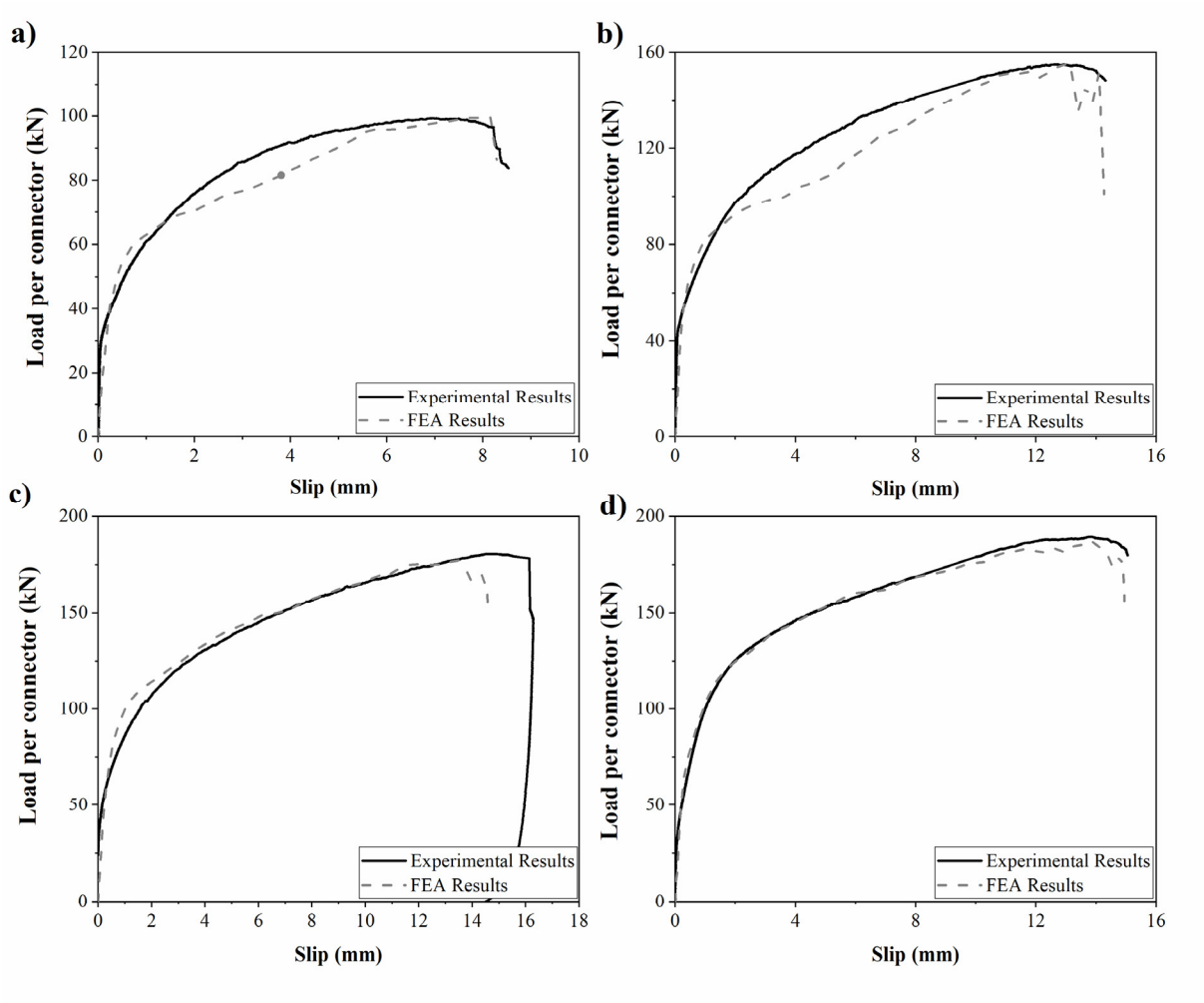

Fig. 9. Comparison of load slip behaviour from experimental tests and FE models for a) Test 7 b) Test 8 c) Test 10 and d) Test 12.

The FE model was also able to predict the actual failure modes of the push-out test specimens. FEA and experimental deformed shapes of bolt connectors are compared in Fig. 10. The FE model was capable to predict the gradual yielding of the bolts as well as the formation of two short length regions of high plasticity, due to combined shear, bending and axial internal stresses. Apart from bolt deflection, extensive concrete crushing was observed in front of the conical nut and the bolt shank at both experimental and numerical results, as shown in Fig.11.

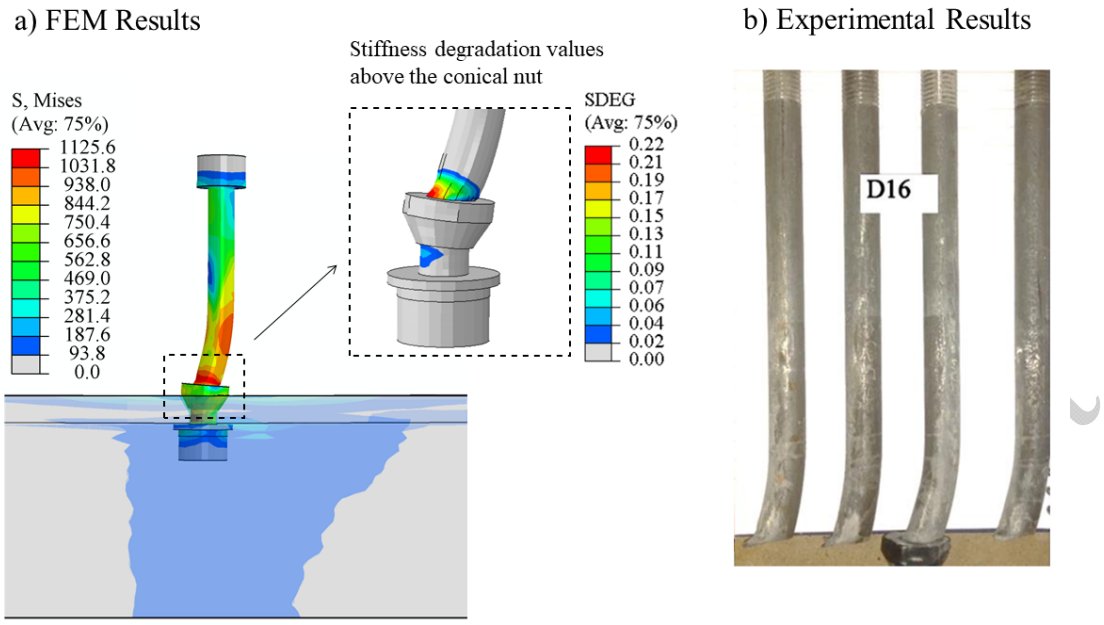

Fig. 10. Deflected shapes of the bolts from push-out test 12.

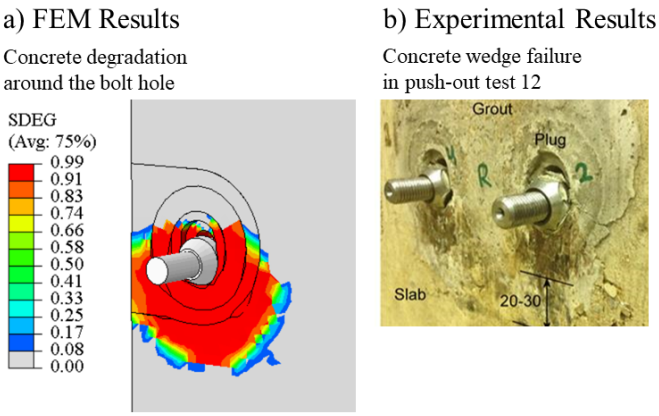

Fig. 11. Concrete wedge failure in push-out test 12.

The FE model was also validated against the experimental results in terms of characteristic resistance, slip capacity and stiffness of the connection and the results are summarized in Table 2. According to Eurocode 4 [33], the characteristic resistance P_{Rk} of the specimens was measured as the minimum failure load (divided by the number of the connectors) reduced by 10%. It was concluded that the FE model was able to predict the characteristic shear resistance of the LNSC specimens with great accuracy; less than 4% difference between numerical and experimental results. The stiffness of the LNSC was defined following the recommendations of Annex A of Eurocode 4 [33] as $0.7P_{Rk}/s$, where s is the slip at a load of $0.7P_{Rk}$. The

characteristic slip capacity of the specimens was defined as the slip measured at the characteristic load level reduced by 10% [33].

Table 2. Comparison of the shear resistance, stiffness and slip capacity captured by the FE models with tests data.

Test Number	Characteristic resistance (kN)			Shear connection stiffness (kN/mm)			Characteristic slip capacity (mm)		
	Experimental Test	FE Model	$P_{Rk,ex}/P_{Rk,FE}$	Experimental Test	FE Model	$k_{sc,exp}/k_{sc,FE}$	Experimental Test	FE Model	$\delta_{uk,exp}/\delta_{uk,FE}$
	$P_{Rk,exp}$	$P_{Rk,FE}$		$k_{sc,exp}$	$k_{sc,FE}$		$\delta_{uk,exp}$	$\delta_{uk,FE}$	
7	92.4	95.9	0.96	65.9	68.5	0.96	6.76	7.01	0.96
8	139.6	139.3	1.00	43.15	40.4	1.07	11.52	11.55	1.00
10	162.7	159.4	1.02	59.44	64.9	0.92	13.05	10.98	1.19
12	170.6	169.1	1.01	73.7	77.4	0.95	11.09	11.66	0.95

3 Parametric studies and Results

The effects of variations in bolt pretension, bolt diameter, bolt height, bolt tensile strength and plugs compressive strength on the shear resistance, slip capacity and stiffness of the LNSC were assessed by carrying out parametric studies. The details of the push-out specimens for the parametric studies are given in Table 3.

Table 3. Details of the push-out specimens for the parametric study

Parameter	**Specimen**	**Bolt diameter (mm)**	**Bolt pretension force (kN)**	**Plugs compressive strength (MPa)**	**Height of bolt connectors (mm)**	**Bolts tensile strength (MPa)**
Bolt diameter	D1	**12**	25	90	125	950
	D2	**14**	25	90	125	950
	D3	**16**	25	90	125	950
	D4	**20**	25	90	125	950
	D5	**22**	25	90	125	950
Bolt pretension force	PF1	16	**25**	90	125	950
	PF2	16	**40**	90	125	950
	PF3	16	**60**	90	125	950
	PF4	16	**80**	90	125	950
Plugs compressive strength	P1	16	25	**50**	125	950
	P2	16	25	**70**	125	950
	P3	16	25	**90**	125	950
Height of bolt connectors	H1	16	25	90	**90**	950
	H2	16	25	90	**100**	950
	H2	16	25	90	**110**	950
	H3	16	25	90	**125**	950
Bolts tensile strength	T1	16	25	90	125	**800**
	T2	16	25	90	125	**865**
	T3	16	25	90	125	**950**
	T4	16	25	90	125	**1115**

3.1 Effect of bolt diameter

Previous experimental studies conducted by Suwaed and Karavasilis [19] have shown that the diameter of the bolts is among the most influential parameters on the structural behaviour of the LNSC. Suwaed and Karavasilis [19] conducted push-out tests on LNSC specimens using M12, M14 and M16 bolts and it was concluded that an increase in the bolt diameter offered higher shear capacity to the specimens. The behaviour of the specimens was also numerically verified and showed that an increase in bolt diameter from 12mm to 16mm, almost doubled both the characteristic shear resistance and slip capacity of the LNSC specimens.

To expand the experimental databank, LNSC specimens with M20 and M22 bolts were also numerically tested and the results are summarized in Table 4. The parametric results revealed that the shear resistance and stiffness of the specimens are considerably increased with increasing the bolt diameter. More specifically, up to approximately 2.5 times increased shear resistance was observed for specimens with 22mm diameter bolts compared to the specimens with 12mm diameter bolts. The slip capacity of the specimens was also affected by increasing the diameter of the bolt connectors above 16mm. As shown in Fig.12, the predominant failure mode of these specimens was the concrete crushing caused by the high bearing stresses in the conical nut -grout, bolt shank - grout and plug - grout interfaces. Both concrete slab and precast concrete plug were excessively damaged and therefore the slip capacity of the specimens was considerably decreased. It should be mentioned that the slip capacity of the specimen D5, where M22 bolts were used as shear connectors, was less than the required slip capacity recommended by Eurocode 4 (i.e. 6 mm) for a ductile shear connector.

A polynomial regression analysis of characteristic shear resistance of the LNSC with different bolt diameters is presented in Fig.14 and Eq. (11) is proposed for calculating the shear resistance of the specimens, where D is the diameter of the bolts in mm.

$$P_{Rk} = -0.985D^2 + 48.1D - 328 \quad (11)$$

Table 4. Effect of bolt diameter on the characteristic shear resistance, stiffness and slip capacity of the LNSC.

Specimen	Bolt Diameter	Shear Resistance	Shear Resistance ratio	Stiffness	Stiffness ratio	Slip capacity	Slip capacity ratio
	(mm)	(kN)	$P_{rk,Di}/P_{rk,D1}$	(kN/mm)	$k_{sc,Di}/k_{sc,D1}$	(mm)	$\delta_{u,Di}/\delta_{u,D1}$
D1	12	95.9	-	83.0	-	8.2	-
D2	14	139.8	1.46	89.3	1.08	14.3	1.74
D3	16	169.1	1.76	116.1	1.40	14.9	1.82
D4	20	216.5	2.26	141.5	1.70	11.9	1.45
D5	22	228.7	2.38	181.5	2.19	7.1	0.87

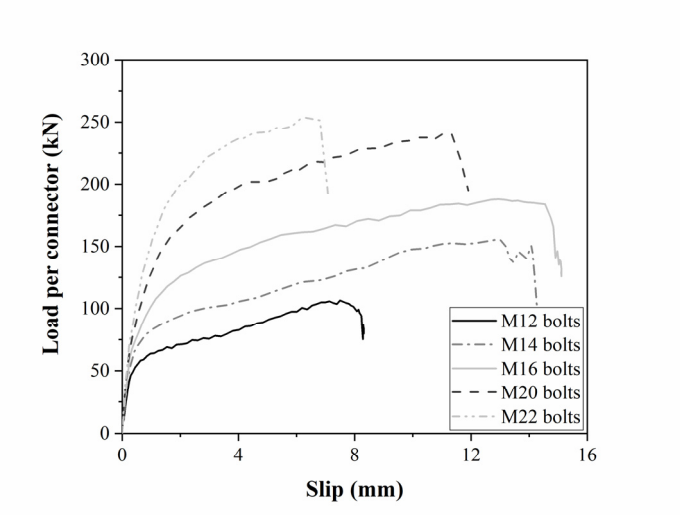

Fig. 12. Effect of bolt diameter on the load-slip response of the LNSC.

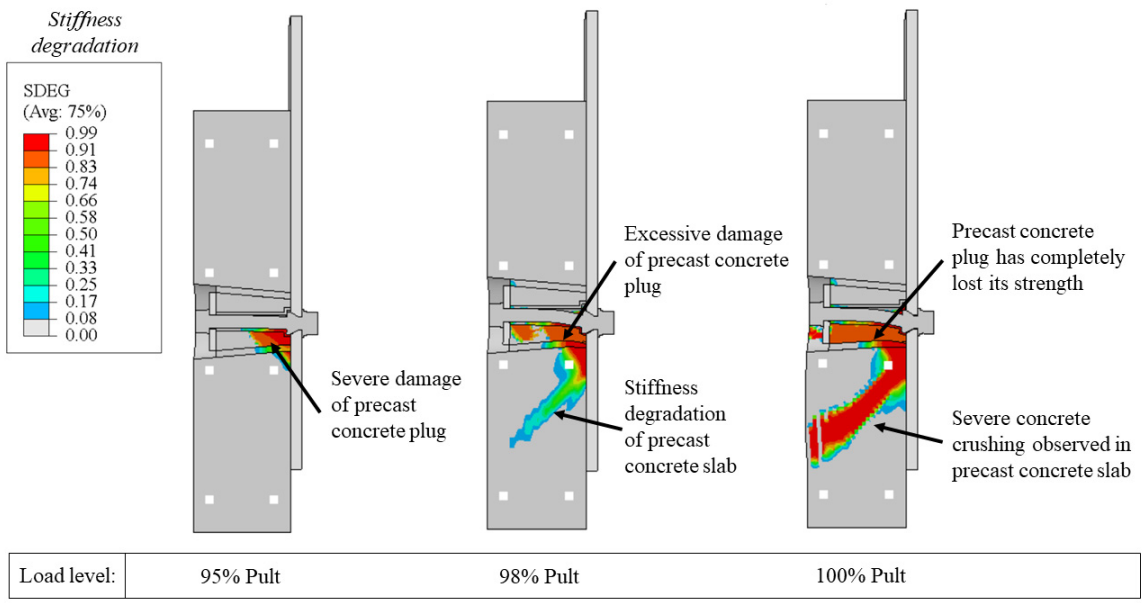

Fig. 13. Concrete failure in specimen D5.

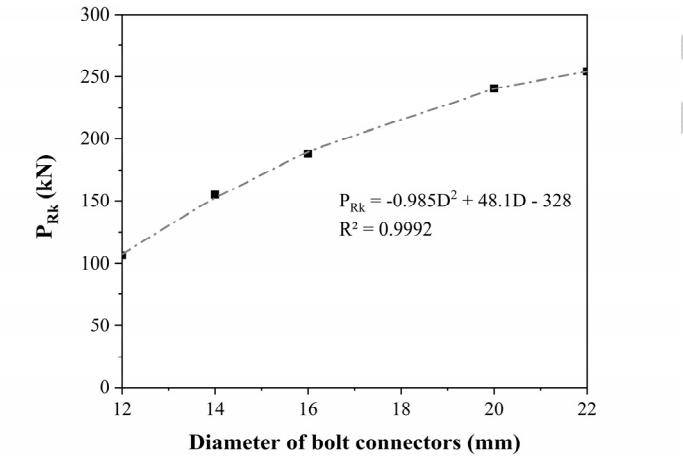

Fig. 14. Effect of bolt diameter on the ultimate resistance of the LNSC.

3.2 Effect of bolt pretension between the conical nut and the upper hexagonal nut

The tightening of the upper hexagonal nut allows the distribution of the load to the connector components through the bolt and the nuts. The results of a parametric study showing the effect of bolt pretension between the conical nut and the upper hexagonal nut on the load-slip behaviour of the LNSC shear connector is illustrated in Fig. 15. The results showed that the bolt pretension did not have any substantial effect on the shear resistance and slip capacity of the specimens. More specifically, the maximum shear resistance and slip capacity increase due to changing the bolt pretension force was less than 2%. However, the bolt pretension force highly affects the stiffness of the specimens, since more than 40% increase of stiffness was observed when the bolt pretension force increased from 25kN to 80kN.

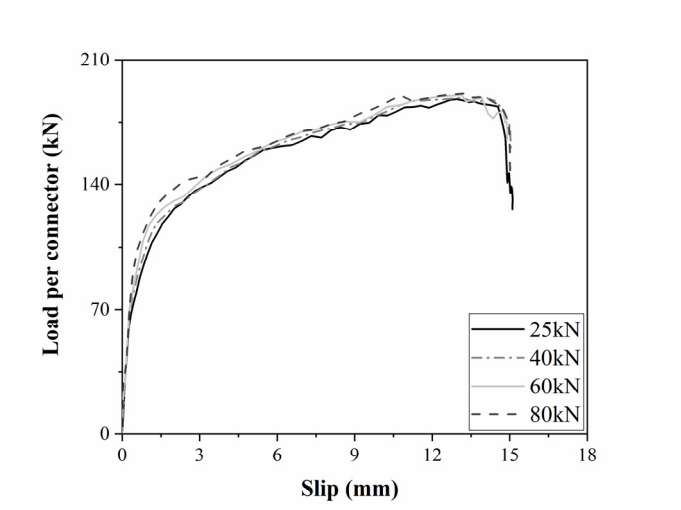

Fig. 15. Effect of bolt pretension on the load-slip response of the LNSC.

3.3 Effect of plugs compressive strength

The load-slip behaviour of the LNSC using precast concrete plugs with different compressive strengths is presented in Fig. 16. The results of the parametric study are summarized in Table 5, where the effect of the plugs compressive strength on the shear resistance, stiffness and slip capacity of the specimens is evaluated. It was concluded that an increase of the plug compressive strength from 50MPa to 70 MPa has a minor influence on the shear resistance,

stiffness and slip capacity of the LNSC specimens. A further increase of the plug's compressive strength to 90 MPa caused a 5% increase on the shear resistance.

Table 5. Effect of plugs compressive strength on the characteristic shear resistance, stiffness and slip capacity of the LNSC.

Specimen	Plugs compressive strength	Shear Resistance	Shear Resistance ratio	Stiffness	Stiffness ratio	Slip capacity	Slip capacity ratio
	(mm)	(kN)	$P_{rk,Pi}/P_{rk,P1}$	(kN/mm)	$k_{sc,Pi}/k_{sc,P1}$	(mm)	$\delta_{u,Pi}/\delta_{u,P1}$
P1	50	159.4	-	108.0	-	14.6	-
P2	70	162.0	1.02	112.5	1.04	14.7	1.00
P3	90	168.1	1.05	116.1	1.07	14.9	1.02

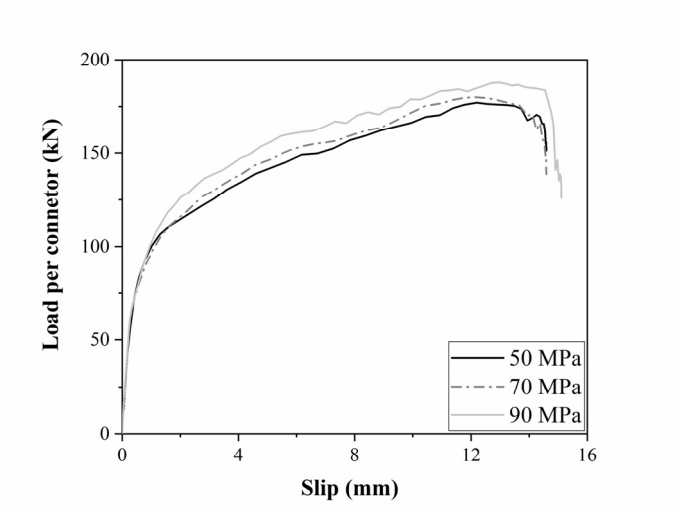

Fig. 16. Effect of plugs compressive strength on the load-slip response of the LNSC.

3.4 Effect of bolt connectors' height to diameter ratio

A parametric study on bolt connectors' height to diameter ratio was contacted using the proposed FE model and the results are summarized in Fig.17 and Table 6. The bolt diameter remained constant (i.e. D=16mm), while the bolt height varied. The results showed that increasing the bolt connector's height increase the shear resistance of the specimens up to 8% but had a minor influence on the slip capacity of the LNSC specimens. A significant increase of the LNSC stiffness was observed when bolts with increased height were used.

Table 6. Effect of bolt connectors height on the characteristic shear resistance, stiffness and slip capacity of the LNSC.

Specimen	h/d ratio	Shear Resistance	Shear Resistance ratio	Stiffness	Stiffness ratio	Slip capacity	Slip capacity ratio
	()	(kN)	$P_{rk,Hi}/P_{rk,H1}$	(kN/mm)	$k_{sc,Hi}/k_{sc,H1}$	(mm)	$\delta_{u,Hi}/\delta_{u,H1}$
H1	6.75	156.1	-	94.3	-	14.7	-
H2	7.25	160.4	1.03	100.1	1.06	14.8	1.01
H3	8	165.1	1.06	105.5	1.21	14.8	1.01
H4	9	169.1	1.08	116.1	1.23	14.8	1.01

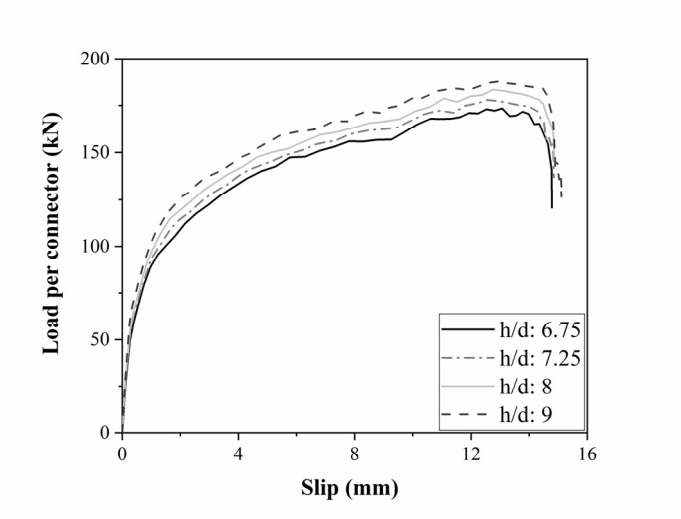

Fig. 17. Effect of bolt connectors' height on the load-slip response of the LNSC.

3.5 Effect of bolts tensile strength

The tensile stress-strain behaviour of the M16 high-strength steel bolts used in the parametric study was defined by using the stress-strain relationship presented in Eq. (12). The relationship is a modification of the model proposed by Mander et al. [34], in order to include the post-peak behaviour of high-strength bolts. The model was verified by comparing the results with experimental data in the available literature [9, 19, 35], and it was concluded that the proposed model with great accuracy, as shown in Fig. 18.

$$f(\varepsilon) = \begin{cases} E\varepsilon, & for\ \varepsilon_y \le \varepsilon < \varepsilon_{sh} \\ \dfrac{f_u - f_y}{1.1 \times (\varepsilon_u - \varepsilon_{sh})} \times (\varepsilon - \varepsilon_y) + f_y, & for\ \varepsilon_y \le \varepsilon < \varepsilon_{sh} \\ f_u - (f_u - f_y) \times \left(\dfrac{\varepsilon_u - \varepsilon}{\varepsilon_u - \varepsilon_{sh}}\right)^{p_1}, & for\ \varepsilon_{sh} \le \varepsilon < \varepsilon_u \\ k - \left[f_f - (f_f - f_u) \times \left(\dfrac{\varepsilon_f - \varepsilon}{\varepsilon_f - \varepsilon_u}\right)^{p_2}\right], & for\ \varepsilon_u \le \varepsilon < \varepsilon_f \end{cases} \quad (12)$$

Where, the stain-hardening strain is defined as: $\varepsilon_{sh} = 0.018 * (f_y/f_u)$ and k, p_1 and p_2 are material parameters defined in Eq. (12-14). The values of stress at fracture f_f and strain at fracture ε_f were calculated based on the available experimental data.

$$p_1 = 2 \times \frac{f_u - f_y}{1.1 \times (\varepsilon_u - \varepsilon_{sh})} \times \frac{\varepsilon_u - \varepsilon_{sh}}{f_u - f_y} \quad (13)$$

$$p_2 = 2 \times \frac{f_f - f_u}{1.1 \times (\varepsilon_f - \varepsilon_u)} \times \frac{\varepsilon_f - \varepsilon_u}{f_f - f_u} \quad (14)$$

$$k = 2 \times \left[\frac{f_f - f_u}{(\varepsilon_f - \varepsilon_u)} \times (\varepsilon - \varepsilon_u) + f_u\right] \quad (15)$$

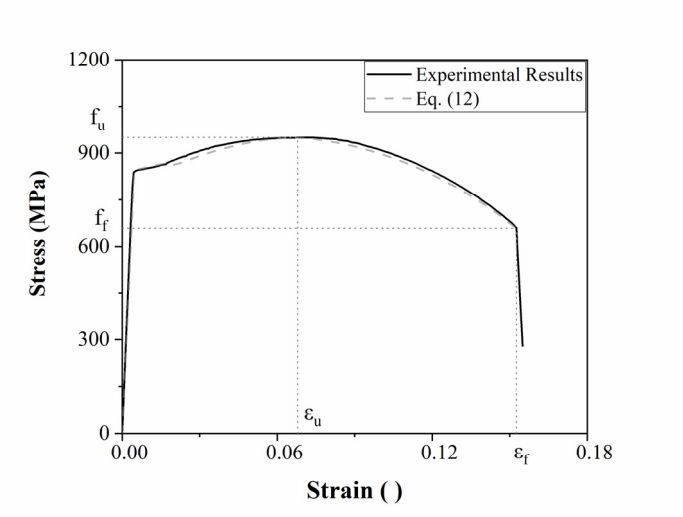

Fig. 18. Comparison between experimental [19] and predicted tensile stress-strain response of high-strength bolt connectors using the proposed modified stress-strain model.

The effect of the tensile strength of the bolt connectors on the load-slip behaviour of the LNSC is illustrated in Fig. 19, while the shear resistance and slip capacity of the specimens are compared in Table 7. The results of the parametric analysis showed that a variation in the tensile strength of the bolts highly affects the overall stress-strain behaviour of the LNSC. Table 7 demonstrates direct correlation between the shear resistance of the LNSC specimens and the tensile strength of bolt connectors. For example, an increase in bolt's tensile strength from 800MPa to 1115MPa, caused a 26% increase of the shear resistance of the specimen. Similarly, both the slip capacity and the stiffness of the specimens were increased by using bolts with high tensile strength.

Table 7. Effect of the yield strength of the bolt connectors on the characteristic shear resistance, stiffness and slip capacity of the LNSC.

Specimen	Bolts tensile strength	Shear Resistance	Shear Resistance ratio	Stiffness	Stiffness ratio	Slip capacity	Slip capacity ratio
	(MPa)	(kN)	$P_{rk,Di}/P_{rk,D1}$	(kN/mm)	$k_{sc,Di}/k_{sc,D1}$	(mm)	$\delta_{u,Di}/\delta_{u,D1}$
B1	800	149.6	-	103.9	-	12.3	-
B2	865	158.6	1.06	107.5	1.03	14.1	1.15
B3	950	168.1	1.13	116.1	1.12	14.9	1.21
B4	1115	188.6	1.26	120.4	1.16	15.7	1.28

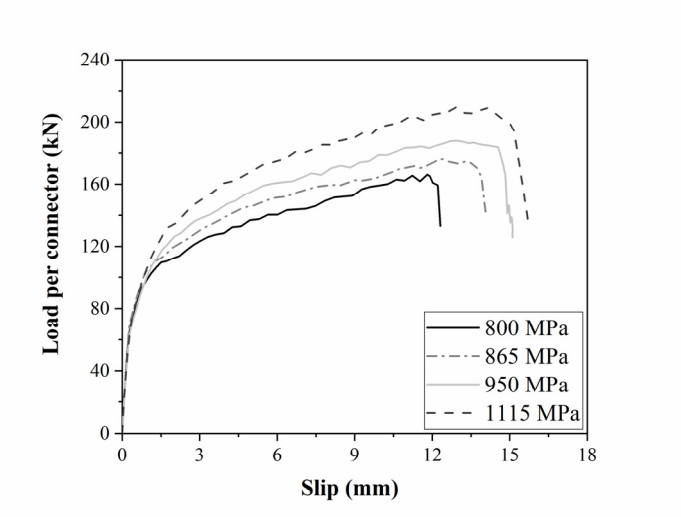

Fig. 19. Effect of tensile strength of bolts on the load-slip response of the LNSC.

4 Design recommendations

The parametric study presented in Clause 3 showed that the tensile strength and the diameter of the bolts highly affect the resistance of the LNSCs. To further study these two parameters, 12 additional parametric tests were conducted, and the results are presented together with the results of the initial parametric study in Table 8. Based on these results, simple design rules to calculate the resistance of the LNSCs are proposed.

Table 8. Effect of bolts diameter and tensile strength on the ultimate resistance of the LNSCs.

Specimen	F_{ult} [kN]	Failure [kN]
M12_T800	87.9	Bolt
M12_T865	95.9	Bolt
M12_T950	105.7	Bolt
M12_T1115	123.6	Bolt
M14_T800	128.8	Bolt
M14_T865	136.3	Bolt
M14_T950	146.0	Bolt
M14_T1115	161.7	Bolt
M16_T800	166.3	Bolt
M16_T865	176.2	Bolt
M16_T950	187.9	Bolt
M16_T1115	209.5	Bolt
M20_T800	222.0	Concrete
M20_T865	231.6	Concrete
M20_T950	241.4	Concrete
M20_T1115	245.2	Concrete
M22_T800	243.9	Concrete
M22_T865	251.9	Concrete
M22_T950	254.7	Concrete
M22_T1115	260.9	Concrete

The initial non-slip behaviour of the LNSCs is attributed to the friction between the steel-concrete plug interfaces. Both bolt pretension force (T) and friction coefficient at the steel-concrete interface (μ) influence the slip resistance of the connector, which can be calculated using Eq. (16). The pretension of the bolts was assumed to be 25kN, according to the experimental work on LNSCs presented by Suwaed and Karavasilis [19]. The coefficient of friction was considered to be equal to 0.5, which is in line with the recommendations of BS 5400-5 [36] for steel-concrete interfaces.

$$F_R = \mu \cdot T \tag{16}$$

For the specimens that failed due bolt fracture, the resistance of the LNSCs obtained from both experimental and numerical analysis was found to be much higher than the pure shear resistance of the bolts, which according to BS EN 1993-1-8 [37] can be calculated using Eq. (17). The increase of the load-bearing capacity of the bolts is attributed to the friction at the steel-concrete plug interface and the inclination of the deflected shape of the bolts.

$$F_s = \alpha_v \cdot f_{ub} \cdot A_s \tag{17}$$

After slip initiation, the bolts gradually elongate in tension. The tensile force F_t can be analysed in two components, one vertical to the steel flange $F_{t,V}$ that increases the tensile force in the bolts and thus increases the clamping action and one horizontal $F_{t,H}$ that coincide with the direction of F_s and therefore increases the bolt resistance to vertical shear. As a result, the resistance of the LNSCs due to friction at this stage can be calculated using Eq. (18).

$$F_{friction} = \mu \cdot F_{t,V} = \mu \cdot F_t \cdot \cos(\beta) \tag{18}$$

Taking all the above into consideration, the resistance of the LNSC is using Eq. (19).

$$F_{R,s} = F_s + F_{friction} + F_{t,H} = 0.6 f_{ub} A_s + F_t \left[\mu \cos(\beta) + \sin(\beta)\right] \tag{19}$$

The values of angle β and the tensile force F_t are shown in

Table 9. The angle β was obtained at the last increment of the analysis prior to specimen failure. The tensile force of the bolts F_t was calculated based on the total force due to contact pressure and frictional stress at the upper hexagonal nut – washer cell interaction. As shown in

Table *9*, the tensile force F_t was on average equal to $0.54 f_{ub} A_s$, while $\mu \cos(\beta) + \sin(\beta)]$ was on average equal to 0.67. Therefore, Eq. (20) can be simply expressed as:

$$F_{R,s} = 0.96 f_{ub} A_s \quad (20)$$

Table 9. Obtained values of the tensile force F_t angle β .

Specimen	F_t	$F_t/(f_{ub}A_s)$	Angle β	μcos(β) + sin(β)
	[kN]	-	[Degrees]	-
M12_T800	49.4	0.54	8.2	0.64
M12_T865	55.9	0.57	8.6	0.64
M12_T950	61.8	0.57	8.8	0.65
M12_T1115	74.4	0.58	9.6	0.66
M14_T800	66.1	0.53	9.6	0.66
M14_T865	71.9	0.53	9.9	0.66
M14_T950	77.1	0.52	10.8	0.68
M14_T1115	94.5	0.54	11.9	0.70
M16_T800	79.9	0.49	11.3	0.69
M16_T865	83.9	0.47	11.6	0.69
M16_T950	110.7	0.57	12.0	0.70
M16_T1115	125.5	0.55	12.5	0.70

The accuracy of Eq. (20) was verified by comparing the predicted ultimate resistance of the LNSCs with the results of the parametric study. As shown in Table 10, the proposed equation was able to predict the resistance of the LNSCs with less than 10% difference.

Table 10. Comparison between the predicted shear resistance of LNSCs using Eq. (20) and the results of the parametric study using the proposed FE model.

Specimen	$F_{ult,FE}$	$F_{R,s}$	$F_{ult,FE} / F_{R,s}$
	[kN]	[kN]	[-]
M12_T800	87.9	86.8	0.99
M12_T865	95.9	93.9	0.98
M12_T950	105.7	103.1	0.98
M12_T1115	123.6	121.0	0.98
M14_T800	128.8	118.2	0.92
M14_T865	136.3	127.8	0.94
M14_T950	146.0	140.3	0.96
M14_T1115	161.7	164.7	1.02
M16_T800	166.3	154.3	0.93
M16_T865	176.2	166.9	0.95
M16_T950	187.9	183.3	0.98

M16_T1115	209.5	215.1	1.03

Eq. (23) proposed by Eurocode 4 [33] was used to predict the resistance of the specimens where concrete failure occurred. In this equation, E_{cm} is the elastic modulus of concrete calculated according to BS EN 1992-1-1, Table 3.1, and f_{ck} is the characteristic cylinder compressive strength of concrete. The compressive strength of the plugs is these specimens was equal to 78 MPa. As shown in Table 11, Eq. (23) was able to predict the resistance of the specimens with a maximum difference of 14%.

$$F_{R,c} = 0.29d^2\sqrt{f_{ck}E_{cm}} \tag{21}$$

Table 11. Comparison between the predicted ultimate resistance of LNSCs using Eq. (23) and the results of the parametric study using the proposed FE model.

Specimen	F_{FE}	$F_{R,c}$	$F_{ult,FE} / F_{R,c}$
	[kN]	[kN]	[-]
M20_T800	222.0	209.8	0.95
M20_T865	231.6	209.8	0.91
M20_T950	241.4	209.8	0.87
M20_T1115	245.2	209.8	0.86
M22_T800	243.9	253.9	1.04
M22_T865	251.9	253.9	1.01
M22_T950	254.7	253.9	1.00
M22_T1115	260.9	253.9	0.97

5 Conclusions

A finite element model of push-out tests has been developed to investigate the shear behaviour of a novel demountable shear connector for steel-concrete composite beams. The results were verified through the use of experimental data available at the literature. The FE model took into account the nonlinear material properties of the components of the shear connector. Material degradation of the different parts of the connector and failure criteria were included in the analysis by using damage models. A quasi-static finite element analysis using dynamic explicit procedure was adopted for the analysis. Extensive parametric studies of push-out specimens with different bolt diameters, bolt pretensions, bolt heights, bolts tensile strength and

compressive strength of plugs were performed using the numerical model. The following conclusions have been drawn:

- The FE model developed in this paper was capable to capture the fundamental behaviour of the shear connector. The shear resistance, stiffness and slip capacity of the shear connector were predicted accurately and compared well with the experimental results available in literature.
- Shear connectors with large diameter bolts achieved higher shear resistance compared to connectors with relatively small diameter. However, the slip capacity of these connectors was noticeably decreased since the predominant mode of failure was shifted from shear failure of bolts to concrete failure due to the extensive damage of the precast concrete plugs.
- By increasing the bolt pretension, the stiffness of the shear connectors was increased. However, the influence of a change in bolt pretension on the shear resistance and slip capacity of the specimens was less noticeable. The same pattern is observed when the plugs compressive strength varies, where only the stiffness of the specimens was slightly affected.
- Increasing the height to diameter ratio of the bolt connectors minimized the damage of the concrete in front of the conical nut and the bolt shank. However, the results showed that the shear resistance was not considerably affected by the height of the connector.
- The tensile strength of the bolts connectors highly affects the shear resistance, the stiffness and the slip capacity of the specimens. It was concluded that bolts with high tensile strength offer better load-slip characteristics to the connection.
- Simple design rules are proposed to calculate the shear resistance of the LNSCs. The resistance was found to be around 20% higher than the corresponding welded studs mainly due to the friction at the steel-concrete interface.

References

[1] Cai, S., Chen, W., Kashani, M.M., Vardanega, P.J., Taylor, C.A. Fatigue life assessment of large scale T-jointed steel truss bridge components. Journal of Constructional Steel Research. 2017; 133: 499-509.

[2] Canning, C., Kashani, M.M. Assessment of U-type wrought iron railway bridges. Proceedings of the Institution of Civil Engineers - Engineering History and Heritage. 2016; 169: (2): 58-67.

[3] Gkoumas, K., Marques Dos Santos, F.L., van Balen, M., Tsakilidis, A., Ortega Hortelano, A., Grosso, M., Haq, G., Pekar, F., Research and Innovation in bridge maintenance, inspection and monitoring, Joint Research Centre (JRC), Luxembrourg: Publications Office of the European Union, 2019.

[4] Tadros, M.K., Baishya, M.C., Rapid replacement of bridge deck, NCHRP Rep. 407, Transportation Research Board, Washington, DC, 1998.

[5] Dallam, L. High strength bolt shear connectors - Pushout tests. ACI Journal. 1968; 65: 767-769.

[6] Dallam, L., Harpster, J., Composite beam tests with high strength bolt shear connectors, Rep. 68-3, Dept. of Civil Engineering, Univ. of Missouri, Columbia, MO, 1968.

[7] Kwon, G., Engelhardt, M.D., Klingner, R.E. Behavior of post-installed shear connectors under static and fatigue loading. Journal of Constructional Steel Research. 2010; 66: (4): 532-541.

[8] Kwon, G., Engelhardt, M.D., Klingner, R.E. Experimental behavior of bridge beams retrofitted with postinstalled shear connectors. Journal of Bridge Engineering. 2011; 16: 536-545.

[9] Pavlović, M., Marković, Z., Veljković, M., Buđevac, D. Bolted shear connectors vs. headed studs behaviour in push-out tests. Journal of Constructional Steel Research. 2013; 88: 134-149.

[10] Dai, X., Lam, D., Saveri, E. Effect of concrete strength and stud collar size to shear capacity of demountable shear connectors. Journal of Structural Engineering. 2015; 141: 04015025

[11] Lee, M.S.S., Bradford, M.A., Sustainable composite beams with deconstructable bolted shear connectors, Taylor & Francis Group, London, 2013.

[12] Rowe, M., Bradford, M.A., Partial Shear Interaction in Deconstructable Steel-Concrete Composite Beams with Bolted Shear Connectors, Design, Fabrication and Economy of Metal Structures, International Conference Proceedings, Miskolc, Hungary, 2013, pp. 585-590.

[13] Bradford, M.A., Pi, Y.-L., Computational Modelling of Deconstructable Composite Steel-Concrete Beams, Proceedings of the Eleventh International Conference on Computational Structures Technology Civil-Comp Press, Stirlingshire, Scotland, 2012.

[14] Ataei, A., Bradford, M.A., FE modelling of sustainable semi-rigid flush end plate composite joints with deconstructable bolted shear connectors, International Conference on Composite Construction in Steel and Concrete, ASCE, Australia, 2014.

[15] Ataei, A., Bradford, M.A., Liu, X. Experimental study of composite beams having a precast geopolymer concrete slab and deconstructable bolted shear connectors. Engineering Structures. 2016; 114: 1-13.

[16] Chen, Y.T., Zhao, Y., West, J.S., Walbridge, S. Behaviour of steel–precast composite girders with through-bolt shear connectors under static loading. Journal of Constructional Steel Research. 2014; 103: 168-178.

[17] Liu, X., Bradford Mark, A., Lee Michael, S.S. Behavior of High-Strength Friction-Grip Bolted Shear Connectors in Sustainable Composite Beams. Journal of Structural Engineering. 2015; 141: (6): 04014149.

[18] Liu, X., Bradford, M.A., Chen, Q.-J., Ban, H. Finite element modelling of steel–concrete composite beams with high-strength friction-grip bolt shear connectors. Finite Elements in Analysis and Design. 2016; 108: 54-65.

[19] Suwaed, A.S., Karavasilis, T.L. Novel demountable shear connector for accelerated disassembly, repair, or replacement of precast steel-concrete composite bridges. Journal of Bridge Engineering. 2017; 22: 04017052.

[20] Yun, X., Gardner, L. Stress-strain curves for hot-rolled steels. Journal of Constructional Steel Research. 2017; 133: 36-46.

[21] Eurocode 2: Design of concrete structures - Part 1-1 : General rules and rules for buildings BS EN 1992-1-1. BSI (British Standards Institution). London; 2004.

[22] Trattnig, G., Antretter, T., Pippan, R. Fracture of austenitic steel subject to a wide range of stress triaxiality ratios and crack deformation modes. Engineering Fracture Mechanics. 2008; 75: (2): 223-235.

[23] Rice, J., Tracey, D. On the ductile enlargement of voids in triaxial stress fields. Journal of the Mechanics and Physics of Solids. 1969; 17: (3): 201-217.

[24] Hillerborg, A., Modéer, M., Petersson, P.E. Analysis of crack formation and crack growth in concrete by means of fracture mechanics and finite elements. Cement and Concrete Research. 1976; 6: (6): 773-781.

[25] Carreira, D., Chu, K. Stress–strain relationship for plain concrete in compression. ACI Journal. 1985; 82: (797-804).

[26] Hsu, L., Hsu, C. Complete stress - strain behaviour of high-strength concrete under compression. Magazine of Concrete Research. 1994; 169: (301-312).

[27] Oehlers, D.J., Bradford, M.A., Elementary behavior of composite steel & concrete structural members, Butterworth-Heinemann, Oxford, 1999.

[28] Papanikolaou, V., Kappos, A. Confinement-sensitive plasticity constitutive model for concrete in triaxial compression. International Journal of Solids and Structures. 2007; 44: 7021–7048.

[29] Yu, T., Teng, J.G., Wong, Y.L., Dong, S.L. Finite element modeling of confined concrete-I: Drucker–Prager type plasticity model. Engineering Structures. 2010; 32: (3): 665-679.

[30] ABAQUS. ABAQUS/CAE User's Manual. Hibbitt, Karlsson & Sorensen, Inc. 2010.

[31] Bažant, Z.P., Becq-Giraudon, E. Statistical prediction of fracture parameters of concrete and implications for choice of testing standard. Cement and Concrete Research. 2002; 32: (4): 529-556.

[32] CEB-FIP Model Code 1990. FIP. London; 1993.

[33] Eurocode 4: Design of composite steel and concrete structures. Part 1-1: General rules and rules for buildings. BS EN 1994-1-1. BSI (British Standards Institution). London; 2004.

[34] Mander, J., Seismic design of bridge piers., Department of Civil Engineering, vol PhD, University of Canterbury,, Christchurch, New Zealand, 1983.

[35] Panga, X., Hua, Y., Tanga, S., Xianga, Z., Wud, G., Xue, T., Wang, X. Physical properties of high-strength bolt materials at elevated temperatures. Results in Physics. 2019; 102156.

[36] Steel, concrete and composite bridges. Part 5: Code of practice for design of composite bridges. BS 5400-5. BSI (British Standards Institution). London; 1979.

[37] UK National Annex to Eurocode 3: Design of steel streuctures, Part 1-8: Design of Joints. NA to EN 1993-1-8. BSI (British Standars Institute). London; 2005.